Title
Electrochemical Investigation of LSGMC-Composite Cathodes on LSGM-Substrate

Journal
ECS Transactions, 13(26)

ISSN
1938-5862

ISBN
9781615672851

Authors
Do, Anh-Tuan
Guo, James
Lu, Xinyu
et al.

Publication Date
2008-12-18

DOI
10.1149/1.3050389

ECS Transactions, 13 (26) 165-180 (2008)
10.1149/1.3050389 ©The Electrochemical Society

Electrochemical Investigation of LSGMC-Composite Cathodes on LSGM-Substrate

Anh-Tuan Do[a], James Guo[a], Xinyu Lu[a], Thomas Pine[a], Joongmyeon Bae[b], Jack Brouwer[a]

[a] National Fuel Cell Research Center, University of California, Irvine, CA 92697-3550

[b] Department of Mechanical Engineering, KAIST, South Korea

As potential intermediate-temperature SOFC cathodes, perovskite composite cathode materials were evaluated in combination with a $La_{0.8}Sr_{0.2}Ga_{0.8}Mg_{0.2}O_{3-\delta}$ (LSGM) electrolyte. Various cathode materials $La_{0.6}Sr_{0.4}Co_{0.2}Fe_{0.8}O_{3-\delta}$ (LSCF), $Ba_{0.5}Sr_{0.5}Co_{0.8}Fe_{0.2}O_{3-\delta}$ (BSCF), and $Pr_{0.3}Sr_{0.7}Co_{0.8}Fe_{0.2}O_{3-\delta}$ (PSCF) were compounded with $La_{0.8}Sr_{0.2}Ga_{0.8}Mg_{0.1}Co_{0.1}O_{3-\delta}$ (LSGMC) as a mixed conducting composite element. All powders were synthesized by the glycine-nitrate process (GNP). XRD analysis found resistive phases of $LaSrGaO_4$ and $LaSrGa_3O_7$ present in the calcined layer of composite cathodes on LSGM. A bulk ohmic resistance of 3.81 $\Omega \cdot cm^2$ and an interfacial resistance value of 0.16 Ω were measured for LSCF/LSGMC composite cathode on LSGM substrate at 800ºC in air. Low-frequency secondary arcs in the impedance spectra of LSCF/LSGMC cathode coupled with low current density and low cathode porosity suggested possible mass transfer limitations. The LSCF/LSGMC composite electrode performed best at 800ºC (0.11 A/cm^2 at 0.045 V overpotential) while the BSCF/LSGMC performed best at the lowest temperature investigated (0.1 A/cm^2 at 700ºC and 0.04 V overpotential).

Introduction

There is a growing interest in reducing the operating temperature of the solid oxide fuel cells (SOFC) from 1000ºC to between 600 and 800ºC (1). A lower operating temperature range can resolve many degradation problems associated with the conventional SOFC operating temperatures, such as nickel catalyst coarsening by the Ostwald ripening mechanism, delamination of the SOFC tri-layer due to thermal stresses, and/or failure of sealant materials. In addition, the lower operating temperature may allow the use of lower cost components such as metal interconnects and balance of plant made from less exotic alloys. There are notable challenges associated with operating a conventional YSZ-based SOFC at intermediate temperature. The most significant is that of insufficient electrolyte conductivity and high cathodic interfacial resistance (i.e. high cathodic activation polarization). The current commercial YSZ electrolyte can achieve ionic conductivity of 0.1 S/cm at 1000ºC but only 0.02 S/cm at 800ºC (2); therefore, it is desirable to find alternative electrolyte and cathode materials for intermediate temperature SOFCs (IT-SOFCs). In recent years, Sr- and Mg-doped $LaGaO_3$ (LSGM)

perovskite materials have gained considerable attention as potential electrolytes for intermediate temperature (IT) SOFCs. Many of the reported LSGM compositions exhibited ionic conductivity at 800ºC (3-6) higher or comparable to that of YSZ at 1000ºC. The highest electrical conductivity, 0.17 S/cm at 800ºC, was achieved with $La_{0.8}Sr_{0.2}Ga_{0.8}Mg_{0.2}O_{3-\delta}$ by Ishihara et al. (7). When LSGM was doped with cobalt (LSGMC) at the Ga site, electrical conductivity as high as 0.43 S/cm at 800ºC was achieved with 15 mol % Co (8). However, electronic conductivity was found by Ishihara et al. to be too high for electrolyte applications when cobalt content was 8.5 mol % or higher (9).

The conventional cathode, Sr-doped $LaMnO_3$ (LSM), has shown good performance for high-temperature SOFC operation (i.e. 900 to 1000ºC) (2); however, LSM becomes almost exclusively an electronic conductor when there is an absence of oxygen vacancies in its structure. This restricts the locations that oxygen can be reduced to the triple-phase boundary (TPB) regions, where air, cathode, and electrolyte are in contact. Therefore, LSM experiences rapidly decreasing performance at lower temperatures (10). This motivates the search for a mixed ionic and electronic conducting (MIEC) oxide that can be used as a cathode material for IT-SOFCs. Several of the potential cathode materials are based on cobalt-containing perovskites such as $Ba_{1-x}Sr_xCo_{1-y}Fe_yO_{3-\delta}$ (BSCF), $La_{1-x}Sr_xCo_{1-y}Fe_yO_{3-\delta}$ (LSCF), $Pr_{1-x}Sr_xCo_{1-y}Fe_yO_{3-\delta}$ (PSCF), and $Sr_{0.5}Sm_{0.5}O_3$ (SSC). These cathode materials in general have good electrical conductivities but high thermal expansion coefficient (TEC) mismatch with the LSGM electrolyte (11-11.5×10^{-6} K^{-1}).

Previous studies on BSCF have shown not only high TEC of 19.7×10^{-6} K^{-1} but also relatively low conductivity of 25.4 S/cm at 800ºC in air for $Ba_{0.5}Sr_{0.5}Co_{0.8}Fe_{0.2}O_{3-\delta}$ (11). Pena-Martinez et al. (12) reported the compatibility of this BSCF composition on a $La_{0.9}Sr_{0.1}Ga_{0.8}Mg_{0.2}O_{2.85}$ electrolyte, but they were only able to achieve a power density of 160 mW/cm^2 at 800ºC. Even though BSCF formed good interfacial contact with the LSGM electrolyte, XRD analysis suggested a surface reaction caused by diffusion of Co above 1000ºC that resulted in high cathode overpotential.

In studying various lanthanide cation-doped cathodes for $Ln_{0.6}Sr_{0.4}Co_{0.2}Fe_{0.8}O_3$ (Ln = La, Pr, Nd, Sm), Xu et al. (13) reported a much higher electrical conductivity for La (~400 S/cm) as compared to Pr (~200 S/cm) at 800ºC. Swierczek and Gozu (14) also reported an electrical conductivity of 315 S/cm at 600ºC for $La_{0.6}Sr_{0.4}Co_{0.2}Fe_{0.8}O_{3-\delta}$, highest amongst tested LSCF perovskites. Moreover, LSCF6428 has been reported as a compatible cathode on an LSGM electrolyte, $La_{0.9}Sr_{0.1}Ga_{0.8}Mg_{0.2}O_{3-\delta}$, reaching a power density as high as 1.05 W/cm^2 at 750ºC (15).

PSCF has also gained considerable attention recently as a possible cathode for IT-SOFCs. Qiu et al. (16) observed that for various doping levels of Fe, the overpotential of $Pr_{1-x}Sr_xCo_{1-y}Fe_yO_{3-\delta}$ (x = 0.2, 0.3) cathodes increased with increasing Fe content from 0 to 0.8. In addition, higher Fe content led to lower TEC, bringing it closer to the TEC of the electrolytes. Alternatively, Kim et al. (17) reported that $Pr_{0.3}Sr_{0.7}Co_{0.3}Fe_{0.7}O_{3-\delta}$ has the lowest ASR value, 0.13 Ω cm^2 with 0.84 eV of activation energy but a high TEC value of 18.9×10^{-6} K^{-1} at 700ºC.

Lv et al. (18) investigated $Sm_{0.5}Sr_{0.5}CoO_{3-\delta}$ (SSC) and found that SSC exhibited electrical conductivity as high as 707 S/cm at 800ºC and a high TEC of 20.5×10^{-6} K^{-1}. Full cell testing of an SSC cathode on electrolyte-supported LSGM with NiO-SDC as the

anode attained a power density of 222 mW/cm^2 at 800ºC (19). Xia et al. (20) reported that the electrochemical performance of an SSC cathode could be further improved by adding samaria-doped ceria (SDC; $Sm_{0.2}Ce_{0.8}O_{1.9}$). SDC not only provides more ionic conducting elements but it also maintains porosity in the cathode by preventing SSC particles from densifying during calcinations and sintering. By testing various composite SSC cathodes, Xia et al. (20) determined that the best performing composite was a 70:30 weight percent SSC:SDC mixture at 600ºC. Qin et al. (21) confirmed that composite cathode SSC/SDC of 7:3 weight ratio narrowly edged out the 6:4 composite as having the lowest ASR at 600ºC. The activation energy of SSC/SDC(6:4) was determined by Baek et al. (22) to be lower than that of SSC/SDC(7:3) (i.e. 0.9 eV versus 0.94 eV, respectively). The authors also found that the TEC value of the 6:4 mixture was lowered to 12.3×10^{-6} K^{-1} at 600ºC. Thus, the SSC/SDC(6:4) might perform better for the temperature range of 600-800ºC.

In this work, we study the performance of LSGMC-compounded cathodes on LSGM electrolytes. The addition of LSGMC as a cathode compounding element serves several purposes. The first is to reduce the TEC mismatch between the cobalt-based cathode materials and LSGM and improve interfacial adhesion. This compounding element also adds electronic conductivity to the cathode thereby increasing the number of triple-phase boundaries (TPBs) and promoting percolation of more ionic pathways to the electrolyte. The cathodes are of selected perovskite materials $La_{0.6}Sr_{0.4}Co_{0.2}Fe_{0.8}O_{3-\delta}$ (LSCF), $Ba_{0.5}Sr_{0.5}Co_{0.8}Fe_{0.2}O_{3-\delta}$ (BSCF), $Pr_{0.3}Sr_{0.7}Co_{0.3}Fe_{0.7}O_{3-\delta}$ (PSCF), and $Sm_{0.5}Sr_{0.5}CoO_{3-\delta}/Sm_{0.2}Ce_{0.8}O_{1.9}$ (SSC-SDC) are each compounded with $La_{0.8}Sr_{0.2}Ga_{0.8}Mg_{0.1}Co_{0.1}O_{3-\delta}$ (LSGMC) at an 8:2 mixing ratio by weight. It is understood that this mixing ratio is below that required for full percolation of the compounding element. This is intentional as each of the perovskite cathode materials studied herein already possess high ionic conductivity.

Experimental

Powder preparation

All powders were synthesized by glycine-nitrate combustion synthesis. The precursor metal nitrates were dissolved in de-ionized water at the desired stoichiometry for each material composition. Glycine was added as a combustion fuel and complexing agent to the nitrate solution in n_{NO3}:$n_{glycine}$ (i.e. molar ratio of nitrate ion to glycine) of 1 to 0.75. The solution was heated to boil off the water. The solution auto-ignited and combusted to yield an ashy product. For the electrolyte, LSGM powder was calcined at 900ºC for 3 h to burn off any residual carbon and resolve any remaining unreacted species. Calcination was followed by a 48 h ball-milling process with plasticizers, binders, and ethanol to break up agglomerates and aid the pellet pressing process. The powder was then dried and uniaxially pressed in a 32 mm cylindrical die under 45.0 MPa then sintered in air at 1450ºC for 4 h. The finished product was a dense pellet with dimensions of 19-21 mm in diameter and ~1 mm in thickness. Cathode powders of BSCF, LSCF, PSCF, SSC-SDC were produced via a similar GNP method and were fired at 1000ºC for 8 h, 1050ºC for 2 h, 1000ºC for 2 h, and 1250ºC for 1 h, respectively. The

LSGMC compounding element of the cathode was sintered as a loose powder at 1400ºC for 4 h to achieve pure perovskite phase. The composite cathode was prepared by mixing respective cathode powder with LSGMC powder in an 8:2 weight ratio and ball-milled with ethanol for 24 h. The resulting mixture was dried and reserved for the screen-printing step.

X-Ray Diffraction (XRD) patterns were collected using a Siemens D5000 x-ray diffractometer with a Ni-filtered CuKα radiation source at 40kV and 30mA at room temperature for material phase characterization. The scans were taken at a 2θ rate of 0.02º/sec over the range of 20-90º. The XRD samples were loose powders of LSGMC and other cathode materials calcined at various temperatures and an LSGM electrolyte substrate pellet sintered at 1400ºC for 4 h. The sintered LSGM pellet was pressed with a 13 mm cylindrical die using powders ground with an agate mortar and pestle. The morphology of the surface of the cross-section of a half-cell of the SSC-SDC/LSGMC interface was examined using scanning electron microscopy (SEM, Zeiss Ultra 55).

Half-cell fabrication

A half-cell arrangement of composite cathode on LSGM electrolyte was used for the electrochemical tests. The electrodes were deposited using screen printing. The cathode ink slurries were prepared by mixing the composite cathode powders (i.e. cathode + LSGMC) in a 1:1 ratio by weight with a pre-mixed solution of 98% alpha-terpineol and 2% Butvar. The ink was painted on the electrolyte using a 1 cm^2 square mask to form the active area. All screen-printed cathodes were fired at 1100ºC in air for 2 h. Platinum paste (Engelhard, A3788A) and gauze (Alfa Aesar, 52 mesh woven from 0.1 mm diameter wired, 99.9%) were used as current collectors in a three-probe configuration as shown in Figure 1. The half cell was then fired at 950ºC for 1 h to cure the paste. Scanning electron microscopy (SEM) was used to analyze the cathode morphology and the quality of the screen-printed composite cathode and also the integrity of the bonding between the screen-printed composite cathode and the electrolyte.

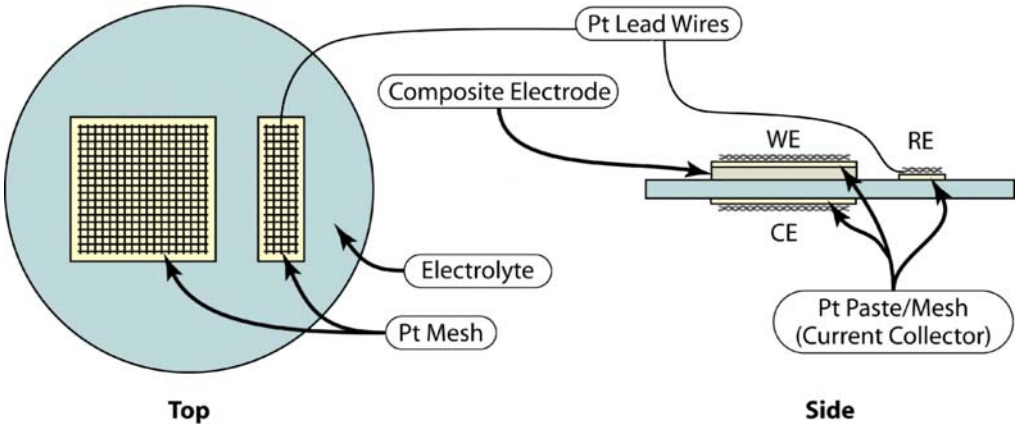

Figure 1. Half cell setup for electrochemical impedance testing.

Electrochemical impedance test

A spring-loaded test rig in combination with the Solartron 1260A frequency analyzer and the 1480A multiplexer potentiostat were used to measure electrochemical characteristics of the half cells. The electrochemical measurements using the electrochemical impedance spectroscopy (EIS) method were taken in air for temperatures of 700, 750, and 800ºC. The impedance was determined at open circuit voltage (OCV) with a frequency range from 0.1 Hz to 100 kHz and 10 mV of ac-amplitude. Cathodic polarization was determined using a *dc*-polarization test with CellTest software to acquire the current-overpotential responses of the half cell.

Results and Discussion

The room temperature XRD patterns of the LSGM pellet and LSGMC powder calcined at various temperatures in air for 4 h are shown in Figure 2. XRD patterns have been identified as the desired perovskite phase with the cubic structure (space group *Pm-3m*) for LSGM (23, 24) and LSGMC (25). The secondary phases of $LaSrGa_3O_7$ (JCPDS # 45-0637) and $LaSrGaO_4$ (# 80-1806) were present in both LSGM and LSGMC samples at the low calcination temperature. Both $LaSrGa_3O_7$ and $LaSrGaO_4$ have been reported as minor phases during the synthesis of LSGM (24, 26) and of LSGMC (27). Neither of the secondary phases is desirable. $LaSrGaO_4$ has been shown to be electrically insulating while the $LaSrGa_3O_7$ phase was reported to have very low electrical conductivity (23). Since Co has been known to improve the sinterability of perovskites, LSGMC specimens demonstrated relatively less secondary phases at 900ºC and 1400ºC as compared to the LSGM. At 1400ºC and 4 h, pure phase perovskite was obtained for LSGMC powders, while small traces of the $LaSrGa_3O_7$ phase still lingered in the LSGM pellets. The LSGM pellets became highly phase pure only after heat treatment up to 1450ºC for 4 h.

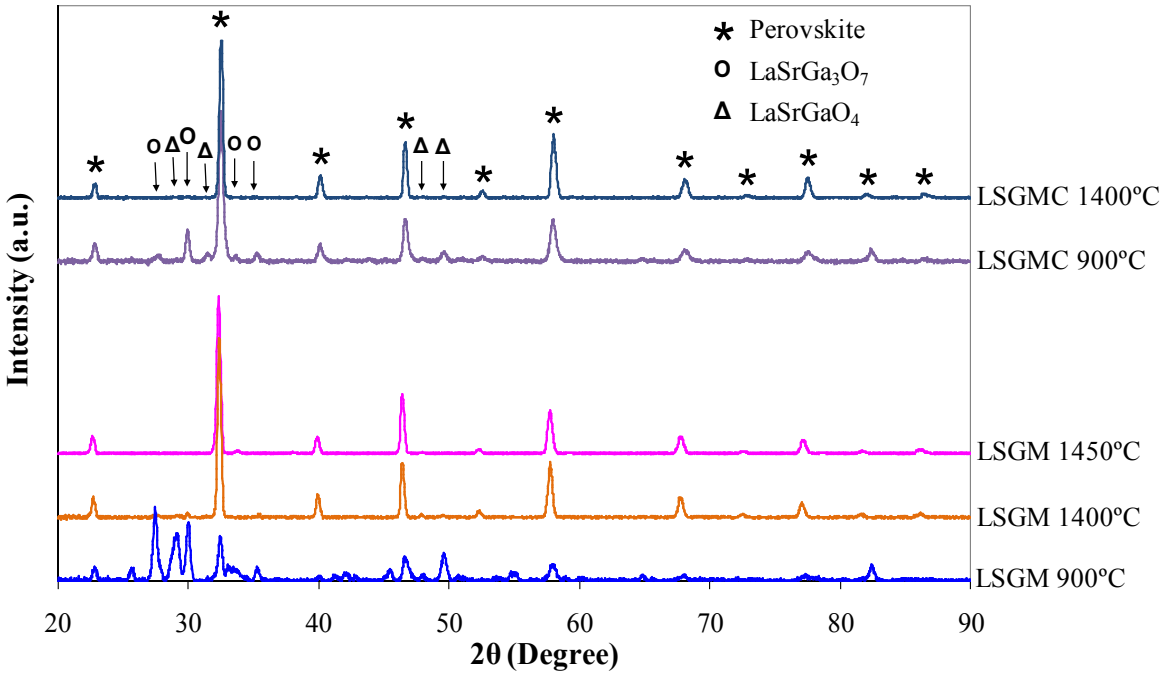

Figure 2. XRD patterns of $La_{0.8}Sr_{0.2}Ga_{0.8}Mg_{0.2}O_{3-\delta}$ (LSGM) pellet and $La_{0.8}Sr_{0.2}Ga_{0.8}Mg_{0.1}Co_{0.1}O_{3-\delta}$ (LSGMC) powders sintered at various temperatures.

The Arrhenius plot of the measured bulk electrical conductivity of LSGM electrolyte as compared to that of 10 mol % YSZ in the literature (1) is shown in Figure 3. The measurements were conducted in air using the *ac*-impedance method with four-probe configuration. The electrolyte pellet used in this test was produced from powders processed by ball-milling with chemical additives to yield an electrical conductivity of 0.10 S/cm at 800ºC.

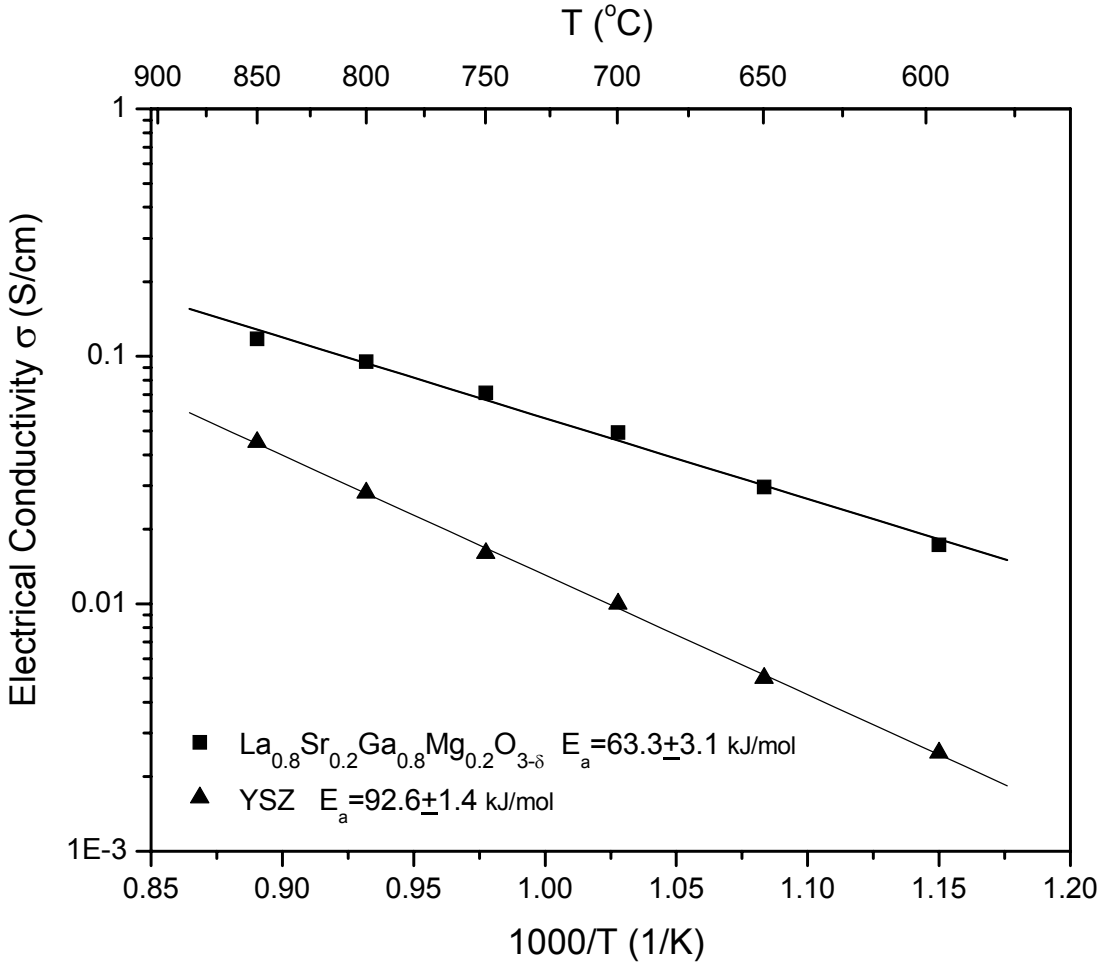

Figure 3. Arrhenius plots of the conductivity of $La_{0.8}Sr_{0.2}Ga_{0.8}Mg_{0.2}O_{3-\delta}$ pellet fabricated from different powder processing methods.

The XRD patterns of calcined BSCF, LSCF, PSCF, and SSC-SDC powders along with the respective patterns of the screen-printed composite cathode on LSGM pellet and of the bare LSGM pellet are displayed in Figure 4 to 7. As can be seen, all cathode powders attained a relatively pure perovskite structure with minimal secondary or impurity phases. The XRD pattern for the BSCF powder agrees well with that reported for $Ba_{0.5}Sr_{0.5}Co_{0.8}Fe_{0.2}O_{3-\delta}$ powder synthesized by the EDTA-Pechini method (i.e. sintered at 1000ºC for 5 h) with the perovskite structure indexed as cubic (space group *Pm-3m*) (11). The scan taken from the LSGM pellet with screen-printed composite BSCF/LSGMC showed a dominant perovskite structure identical to that of the LSGM and also small traces of secondary phases of $LaSrGaO_4$ and $LaSrGa_3O_7$. This suggests possible reaction of LSGM with the cathode due to interdiffusion of cations between the cathode and the electrolyte. Huang et al. (28) have observed precipitation of $LaSrGaO_4$ and $LaSrGa_3O_7$ in LSGM. They attributed this to La diffusion across the electrode/electrolyte interface resulting in La enrichment or depletion in LSGM. Another possible chemical reactivity is Co diffusion into LSGM as reported by Nauomidis et al. using EDS analysis of various Co-based cathode materials on $La_{0.9}Sr_{0.1}Ga_{0.8}Mg_{0.2}O_{3-\delta}$. Extensive Co diffusion is not expected between the cathode materials and the compounding element LSGMC because the Co is already present in the LSGMC. The XRD pattern of LSCF matches that of a cubic structure (space group *Pm-3m*) as reported

by Swierczek and Gozu (14). Figure 5 indicates that the composite LSCF cathode on a LSGM pellet has identical peaks to both LSCF and LSGM due to similar lattice constants of these two perovskites. Peaks of $LaSrGaO_4$ were detected in the composite cathode XRD pattern but not for $LaSrGa_3O_7$. This agrees with observations of Lin and Barnet, (15) which also had trace presence of $LaSrGaO_4$ in a fired LSCF/LSGM powder mixture, but the authors were able to prove by XRD analysis that La diffusion did not take place. This suggests that Co diffusion may be the main reason for $LaSrGaO_4$ precipitation. Single perovskite phase with orthorhombic structure was identified for PSCF powder (Figure 6), which is in agreement with the work of Qiu et al. (16). PSCF and LSGM peaks showed up as distinct peaks in the XRD pattern of composite PSCF/LSGMC on a LSGM pellet. $LaSrGaO_4$ and $LaSrGa_3O_7$ phases again were present in small amount. The XRD scan of the composite SSC-SDC powder gave the expected peaks associated with SSC and SDC (20). There were $LaSrGaO_4$ and $LaSrGa_3O_7$ precipitates detected when the composite cathode SSC-SDC/LSGMC was calcined on LSGM. La diffusion into CeO_2-based materials is strongly suspected in this case due to previous research (28). Possible La diffusion into SSC-SDC powder could stem from LSGMC powder or LSGM pellet and could lead to a La deficiency in the LSGM phase. La deficiency gives rise to the resistive phase $LaSrGa_3O_7$ according to the phase diagram of LSGM. The detection of these insulating phases of $LaSrGaO_4$ and $LaSrGa_3O_7$ could increase the cathodic polarization in all the half cells tested herein.

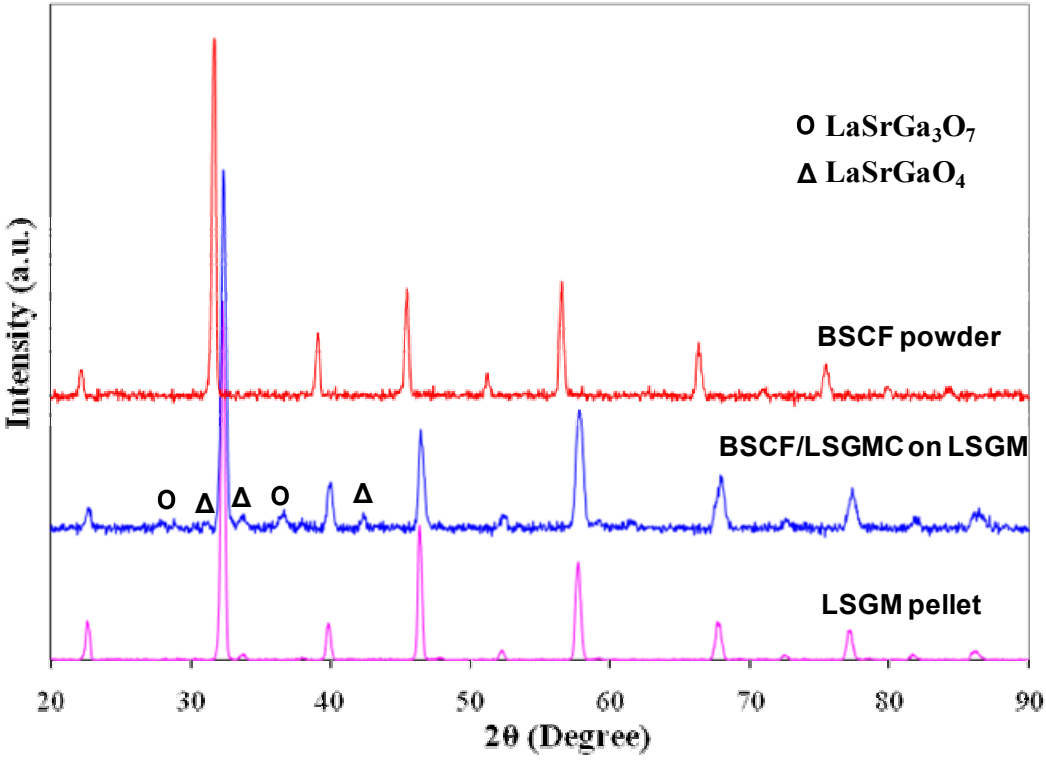

Figure 4. XRD patterns of $Ba_{0.5}Sr_{0.5}Co_{0.8}Fe_{0.2}O_{3-\delta}$ (BSCF, fired at 1000ºC 8h) powder, composite BSCF and $La_{0.8}Sr_{0.2}Ga_{0.8}Mg_{0.1}Co_{0.1}O_{3-\delta}$ (BSCF/LSGMC, sintered at 1100ºC 2h) of 8:2 weight ratio on a LSGM pellet, and a $La_{0.8}Sr_{0.2}Ga_{0.8}Mg_{0.2}O_{3-\delta}$ (LSGM, sintered at 1450ºC 4h) pellet.

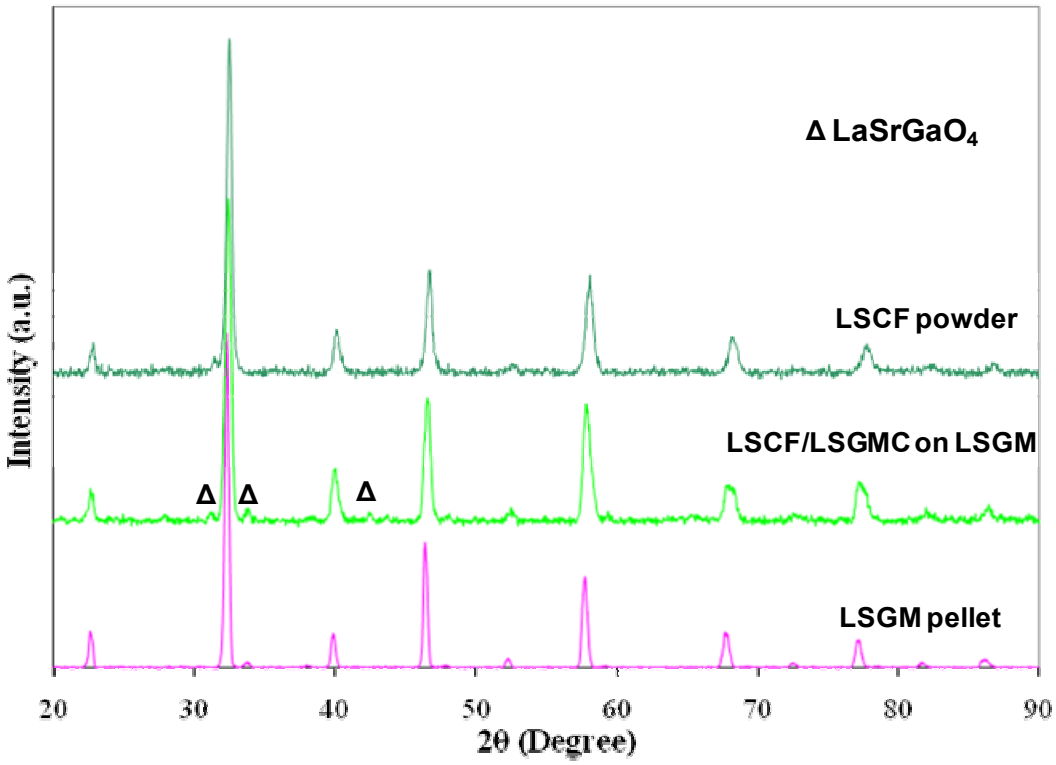

Figure 5. XRD patterns of $La_{0.6}Sr_{0.4}Co_{0.2}Fe_{0.8}O_{3-\delta}$ (LSCF, fired at 1050ºC 2h) powder, composite LSCF/LSGMC(8:2) (sintered at 1100ºC 2h) on a LSGM pellet, and a LSGM pellet (sintered at 1450ºC 4h).

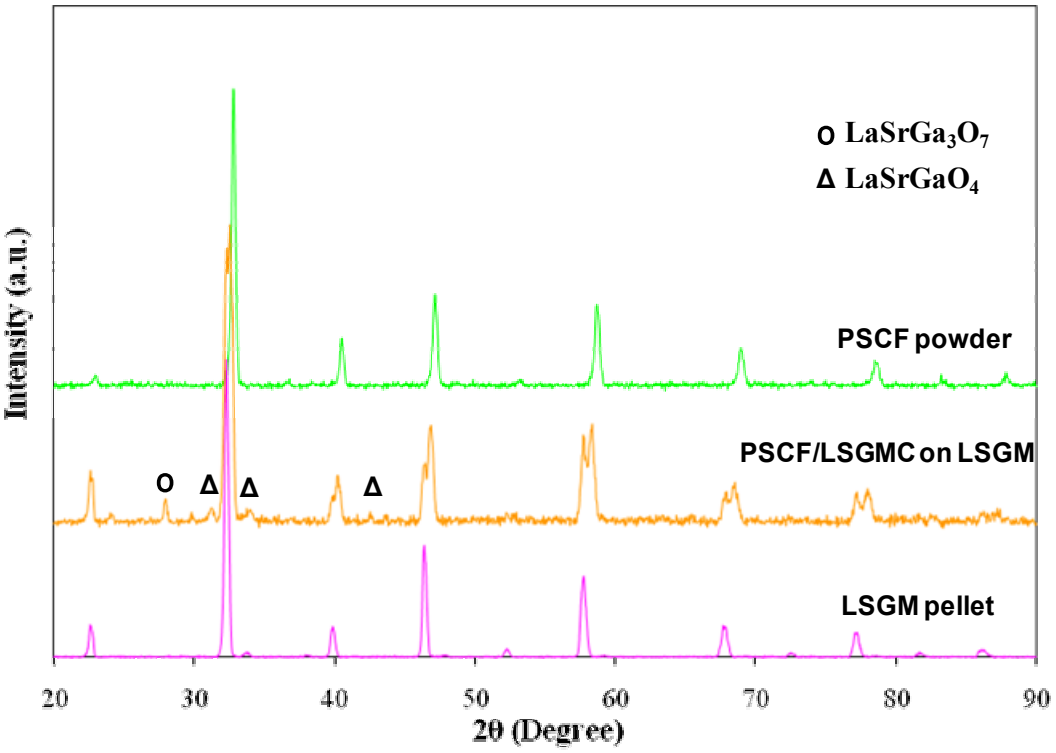

Figure 6. XRD patterns of $Pr_{0.3}Sr_{0.7}Co_{0.3}Fe_{0.7}O_{3-\delta}$ (PSCF, fired at 1000ºC 2 h) powder, composite PSCF/LSGMC(8:2) (sintered at 1100ºC 2h) on a LSGM pellet, and a LSGM pellet (sintered at 1450ºC 4h).

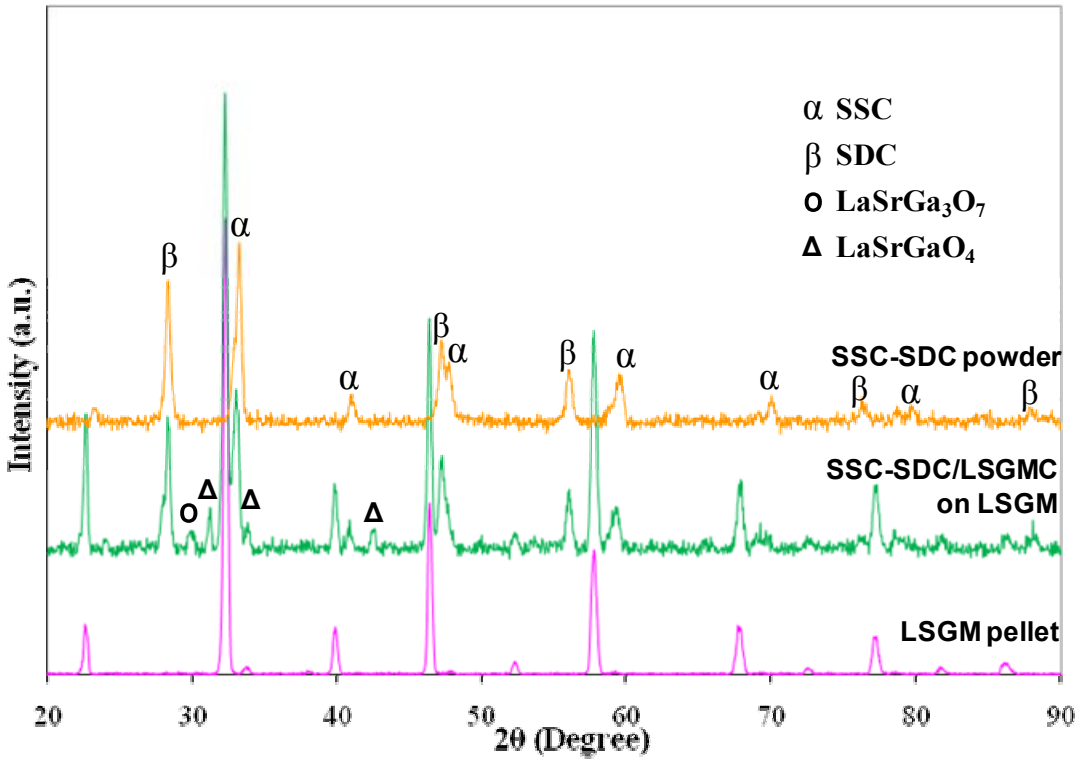

Figure 7. XRD patterns of $Sm_{0.5}Sr_{0.5}CoO_{3-\delta}$/$Sm_{0.2}Ce_{0.8}O_{1.9}$ (SSC-SDC, fired at 1250ºC 1h) powder, composite SSC-SDC/LSGMC(8:2) (sintered at 1100ºC 2h) on a LSGM pellet, and a LSGM pellet (sintered at 1450ºC 4h).

SEM images of the cross-section of a half cell of composite cathode SSC-SDC/LSGMC on a LSGM electrolyte after the electrochemical tests are displayed in Figure 8. The images show a dense and homogeneous phase LSGM electrolyte was produced and that good interfacial contact with porous cathode layer was achieved. The screen-printed cathode layer was about 5-6 μm thick with a fine particle size (<1 μm). The cathode does, however, appear to have low porosity and significant particle agglomeration. This is in agreement with a recent study by Bansal and Zhong (29), which reported that combustion-synthesized SSC powders become increasingly dense when fired as loose powders at temperatures greater than 1000ºC. Cathode porosity in this study was introduced not only by the deposition of the slurry through the porous screen but also by the pyrolysis of organic binder and solvents from the cathode slurry at sintering temperatures. Random integration of already sintered-LSGMC powder amongst calcined-SSC powder in the composite cathode should help hinder extensive diffusion and agglomeration. On the other hand, the low porosity level could also be due to a poor quality binder used in suspending cathode particles in the slurry used for screen-printing. An ink slurry mixture with too low viscosity and binding strength will result in powder particles with more fluid characteristics and higher diffusion at sintering temperatures. Future studies will focus some attention on optimizing the cathode performance by improving the porosity level of the cathodes.

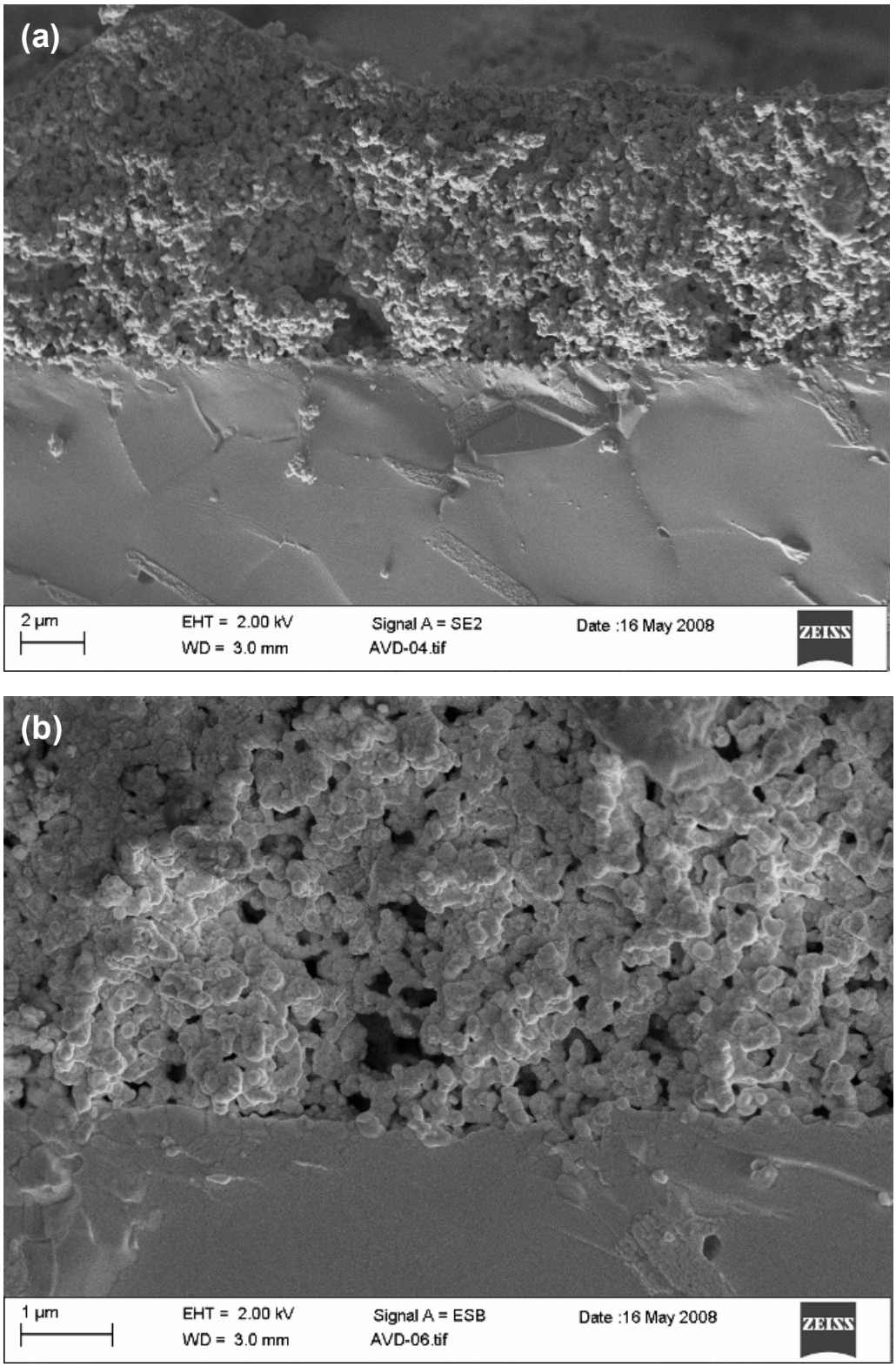

Figure 8. SEM images of the electrode/electrolyte interface for the SSC-SDC/LSGMC cathode half cell in (a) secondary electron mode (b) back-scattered mode.

Figure 9a presents Nyquist plots of the interfacial impedance of composite cathode LSCF:LSGMC (8:2) on LSGM electrolyte as measured in air under open circuit conditions at three temperatures 700, 750, and 800ºC. Bulk ohmic resistance is reduced

from 5.82 Ω (with 1 cm^2 active cathode area) at 700ºC to 3.81 Ω at 800ºC. The interfacial resistance also decreases with higher operating temperature as evidenced by the smaller magnitudes arcs in the high temperature Nyquist plots of Figure 9b. The polarization resistance at 800ºC (0.16 Ω) is more than an order of magnitude higher than that reported for composite cathode $La_{0.6}Sr_{0.4}Co_{0.2}Fe_{0.8}O_{3-\delta}/La_{0.9}Sr_{0.1}Ga_{0.8}Mg_{0.2}O_{3-\delta}$ of a 7:3 weight ratio on LSGM measured in air under OCV conditions at 800ºC by Lin and Barnett (15).

Smaller secondary arcs at low frequency are observed for the impedance spectra measured at 700 and 800ºC. These arcs could be due to the mass transfer limitations in the composite cathode. Mass transfer limitations might be present in the current work due to several possible factors. First, the cathode porosity might not be adequate for the relatively fast surface exchange of O_2. Low porosity or non-percolating pores could lead to insufficient O_2 transport to the reactive sites. Second, reactions between or amongst phases present in the interface may have occurred (e.g. by interdiffusion of La or Co) as implied by the XRD results. Even though the SEM images (Figure 8) indicate no noticeable phase separation for both the cathodes, different phases could have similar *Z* numbers that do not show up on back-scattered mode. Thus, more accurate chemical phase analysis of the cathode/electrolyte interface is needed to verify this possibility.

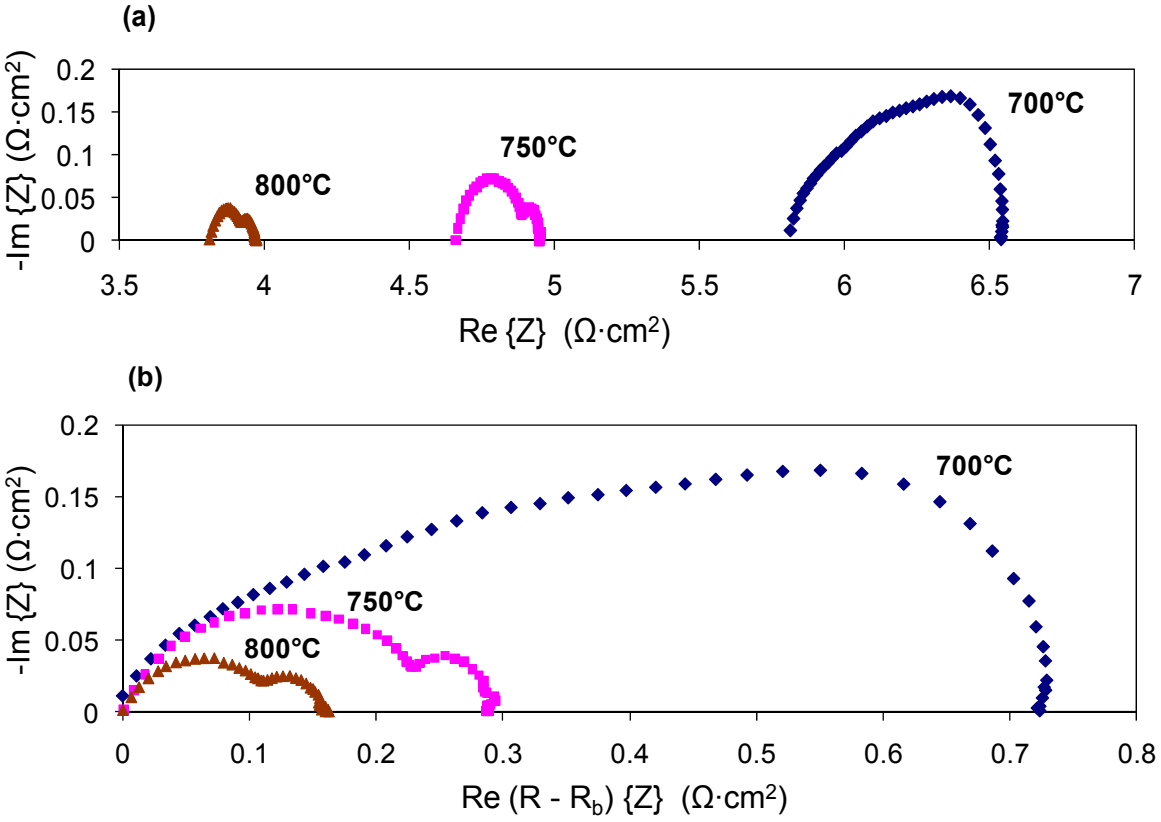

Figure 9. Impedance spectra of composite cathode LSCF/LSGMC on LSGM electrolyte measured at 700, 750, and 800ºC (a) and normalized with Rb removed (b).

The cathodic polarization curves measured at three temperatures 700, 750, and 800ºC for the composite cathode LSCF/LSGMC half-cell is displayed in Figure 10. The composite cathode, calcined at 1100ºC for 2 h, shows the expected temperature dependent behavior of increasing current density for a given overpotential value with

increasing temperature. The polarization curves of the other composite cathode half cells also show the same temperature dependent behavior. Higher overpotential values registered measuring errors for all four composite cathode specimens signifying measurement interference for the cathode/electrolyte interfaces. This is possibly due to the mass transfer limitations or the presence of the resistive $LaSrGaO_4$ and $LaSrGa_3O_7$ phases. The LSCF/LSGMC composite with the lowest observed amount of $LaSrGaO_4$ in its XRD pattern demonstrated the highest current density improvement with temperature for a given overpotential value.

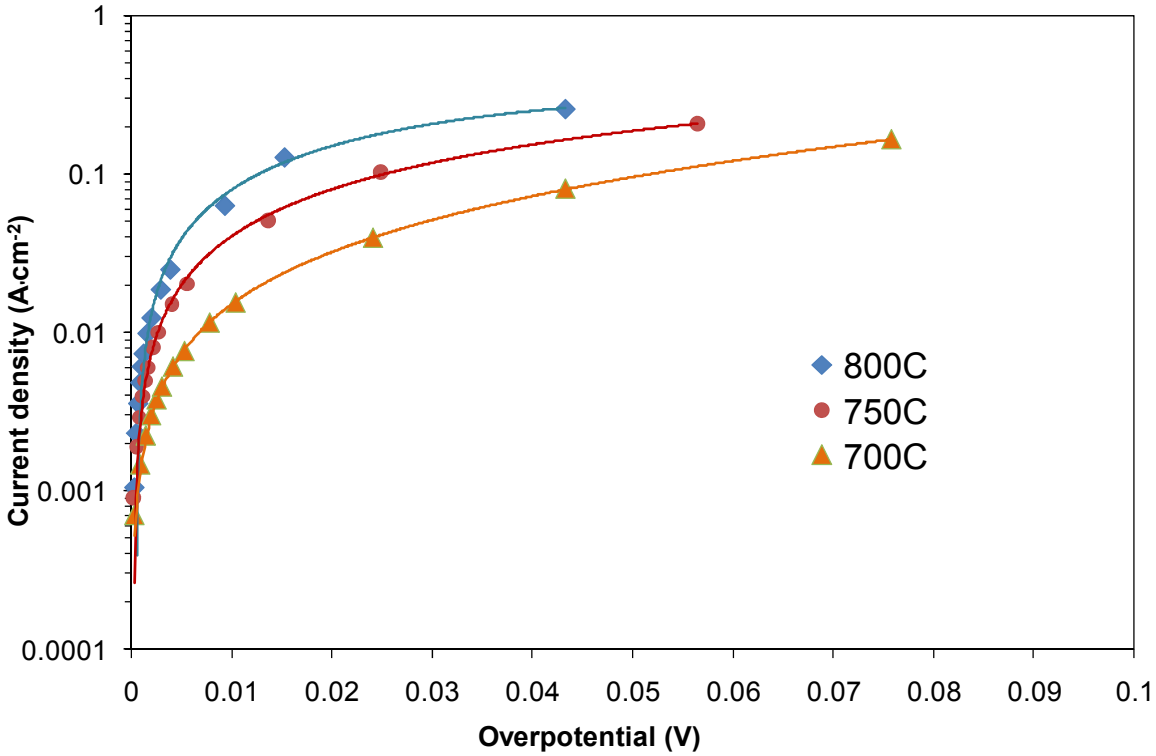

Figure 10. Cathodic polarization curves measured at 700, 750, and 800ºC for composite cathode LSCF/LSGMC on LSGM electrolyte.

Figure 11 provides a performance comparison for the four composite cathodes at each temperature of 700, 750, and 800ºC. At 700ºC, BSCF composite cathode has the best performance with the highest current density at each overpotential, achieving 0.1 $A \cdot cm^{-2}$ at 0.04 V overpotential. BSCF and LSCF composite cathodes showed good performance at 750ºC with both achieving 0.105 $A \cdot cm^{-2}$ at 0.04 V overpotential. The LSCF half cell was found to have a steeper slope in the Tafel region of the polarization curve, indicating that better performance maybe have been possible if higher overpotentials and current densities could have been achieved. The LSCF composite cathode showed the highest performance at 800ºC achieving 0.11 $A \cdot cm^{-2}$at 0.045 V overpotential. The measured performance for PSCF was better than that reported in the literature. CGO-based cells using $Pr_{0.8}Sr_{0.2}Co_{0.8}Fe_{0.2}O_{3-\delta}$ as a cathode by Qiu et al. (16) found a cathodic overpotential as great as 0.16 V for a current density of 0.016 $A \cdot cm^{-2}$ at 700ºC, which is much higher than the measured 0.025 V for this study for $Pr_{0.3}Sr_{0.7}Co_{0.3}Fe_{0.7}O_{3-\delta}$ on LSGM electrolyte.

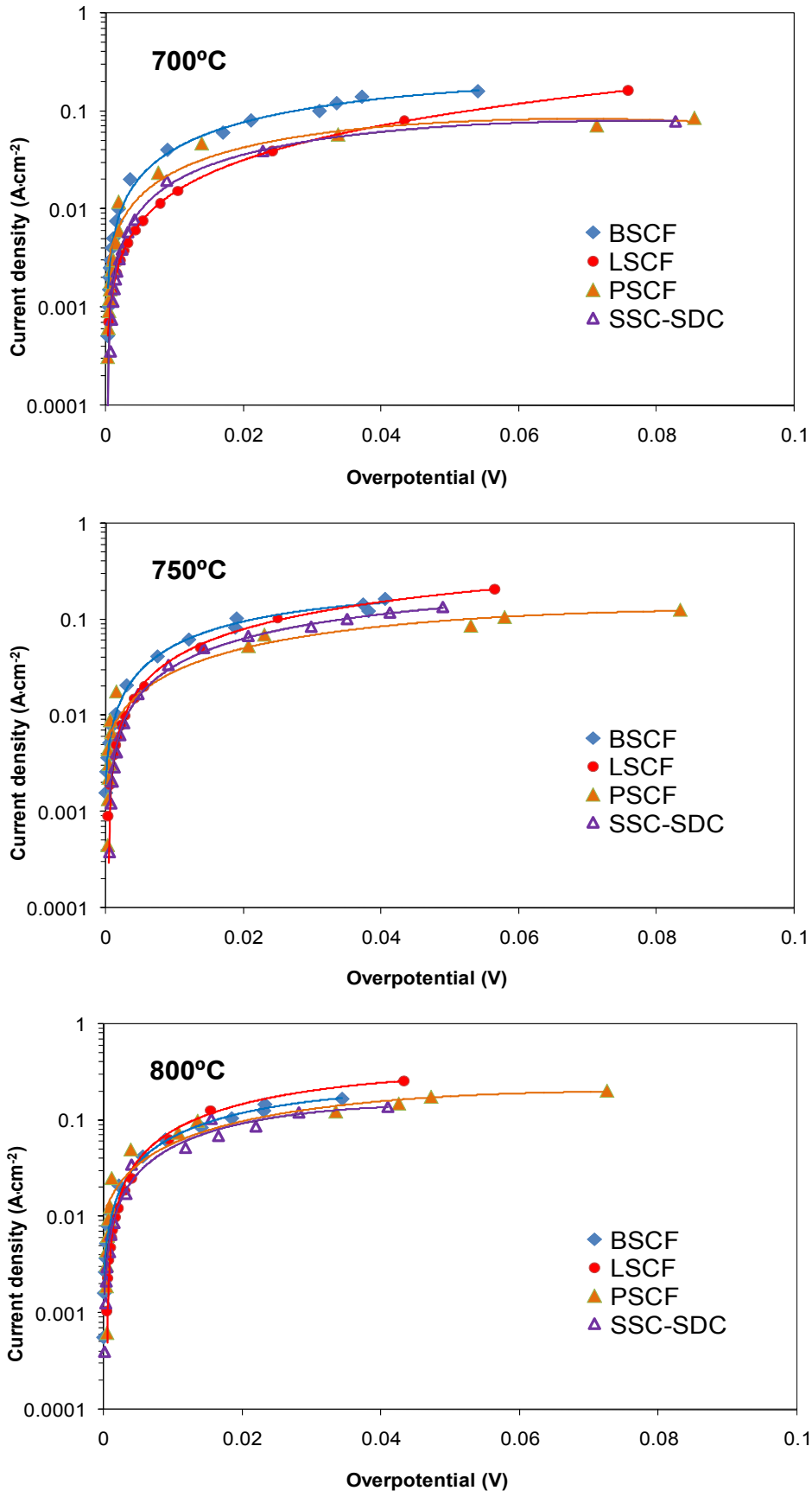

Figure 11. Polarization plots of composite cathodes BSCF, LSCF, PSCF, and SSC-SDC with LSGMC (8:2) tested at 700, 750, and 800ºC.

Conclusion

Glycine-nitrate combustion synthesis has been applied to obtain pure phase perovskite powders of various types for use in composite cathodes for SOFCs. Dense LSGM electrolyte substrates were manufactured with electrical conductivity measured at 0.102 S/cm at 800ºC. Composite cathode materials were obtained by mixing sintered-LSGMC powders with each cathode material in an 8 to 2 weight ratio for both introducing MIEC properties and lowering the TEC. It was found that undesirable phase of $LaSrGaO_4$ and $LaSrGa_3O_7$ were present in the calcined layer of the composite cathodes on LSGM for all four of the tested cathode materials. EIS and *dc*-polarization tests were applied to characterize the cathode/electrolyte interface. Bulk ohmic resistance was measured for LSCF/LSGMC composite cathode giving values of 5.82 $\Omega \cdot cm^2$ and 3.81 $\Omega \cdot cm^2$ at 700 and 800ºC, respectively. An interfacial resistance value of 0.16 Ω at 800ºC was measured for LSCF/LSGMC composite on a LSGM pellet under OCV conditions. DC polarization measurements demonstrated that BSCF/LSGMC composite performed best at 700ºC, while LSCF/LSGMC composite has the best performance at 800ºC. The secondary arcs in the impedance spectra measured for LSCF/LSGMC along with the relatively low current density measured indicate some mass transfer limitations in the composite cathodes. Future work should focus on optimizing the porosity level in the cathode and the firing conditions of screen-printed composite cathodes on LSGM to minimize chemical reactivity of the cathodes with LSGM, and to eliminate resistive phase impurities.

Acknowledgements

The authors acknowledge the financial support of the Fuel Cell Program of the United States Department of Defense.

References

1. S. C. Singhal and K. Kendall, *High temperature solid oxide fuel cells : fundamentals, design, and applications*, p. xvi, Elsevier, Oxford ; New York (2003).
2. J. Larminie and A. Dicks, *Fuel Cell Systems Explained*, p. 400, John Wiley & Sons Ltd. (2003).
3. T. Ishihara, H. Matsuda and Y. Takita, *Journal of the American Chemical Society*, **116**, 3801 (1994).
4. M. Feng and J. B. Goodenough, *European Journal of Solid State and Inorganic Chemistry*, **31**, 663 (1994).
5. M. Shi, N. Liu, Y. D. Xu, Y. P. Yuan, P. Majewski and F. Aldinger, *Journal of Alloys and Compounds*, **425**, 348 (2006).
6. K. Q. Huang, R. S. Tichy and J. B. Goodenough, *Journal of the American Ceramic Society*, **81**, 2565 (1998).
7. T. Ishihara, H. Matsuda and Y. Takita, *Solid State Ionics*, **79**, 147 (1995).
8. T. Ishihara, H. Furutani, M. Honda, T. Yamada, T. Shibayama, T. Akbay, N. Sakai, H. Yokokawa and Y. Takita, *Chemistry of Materials*, **11**, 2081 (1999).
9. T. Ishihara, S. Ishikawa, C. Y. Yu, T. Akbay, K. Hosoi, H. Nishiguchi and Y. Takita, *Physical Chemistry Chemical Physics*, **5**, 2257 (2003).

10. J. M. Ralph, A. C. Schoeler and M. Krumpelt, *Journal of Materials Science*, **36**, 1161 (2001).
11. B. Wei, Z. Lu, S. Y. Li, Y. Q. Liu, K. Y. Liu and W. H. Su, *Electrochemical and Solid State Letters*, **8**, A428 (2005).
12. J. Pena-Martinez, D. Marrero-Lopez, J. C. Ruiz-Morales, B. E. Buergler, P. Nunez and L. J. Gauckler, *Solid State Ionics*, **177**, 2143 (2006).
13. Q. Xu, D. P. Huang, W. Chen, F. Zhang and B. T. Wang, *Journal of Alloys and Compounds*, **429**, 34 (2007).
14. K. Swierczek and M. Gozu, *Journal of Power Sources*, **173**, 695 (2007).
15. Y. Lin and S. A. Barnett, *Solid State Ionics*, **179**, 420 (2008).
16. L. Qiu, T. Ichikawa, A. Hirano, N. Imanishi and Y. Takeda, *Solid State Ionics*, **158**, 55 (2003).
17. J. H. Kim, S.-W. Baek, C. Lee, K. Park and J. Bae, *Solid State Ionics*, **In Press, Corrected Proof** (2008).
18. H. Lv, Y. J. Wu, B. Huang, B. Y. Zhao and K. A. Hu, *Solid State Ionics*, **177**, 901 (2006).
19. S. Yang, T. He and Q. He, *Journal of Alloys and Compounds*, **450**, 400 (2008).
20. C. R. Xia, W. Rauch, F. L. Chen and M. L. Liu, *Solid State Ionics*, **149**, 11 (2002).
21. G. Y. Qin, X. Y. Lu, J. Brouwer and D. R. Mumm, *Solid Oxide Fuel Cells X, Volume 7*, 329 (2007).
22. S.-W. Baek, C. Lee and J. Bae, *Proceedings of FuelCell2007* (2007).
23. M. Rozumek, P. Majewski, H. Schluckwerder, F. Aldinger, K. Kunstler and G. Tomandl, *Journal of the American Ceramic Society*, **87**, 1795 (2004).
24. T. Shibasaki, T. Furuya, S. R. Wang and T. Hashimoto, *Solid State Ionics*, **174**, 193 (2004).
25. K. Kuroda, I. Hashimoto, K. Adachi, J. Akikusa, Y. Tamou, N. Komada, T. Ishihara and Y. Takita, *Solid State Ionics*, **132**, 199 (2000).
26. C. Oncel, B. Ozkaya and M. A. Gulgun, *Journal of the European Ceramic Society*, **27**, 599 (2007).
27. B. A. Khorkounov, H. Nafe and F. Aldinger, *Journal of Solid State Electrochemistry*, **10**, 479 (2006).
28. K. Q. Huang, J. H. Wan and J. B. Goodenough, *Journal of the Electrochemical Society*, **148**, A788 (2001).
29. N. P. Bansal and Z. M. Zhong, *Journal of Power Sources*, **158**, 148 (2006).